Changes in the surface hydrophobicity degree of a MCM-41 used as iron support: a pathway to improve the activity and the olefins production in the Fischer–Tropsch synthesis

N. A. Fellenz, J. F. Bengoa, M. V. Cagnoli & S. G. Marchetti

Journal of Porous Materials

ISSN 1380-2224

J Porous Mater
DOI 10.1007/s10934-016-0342-5

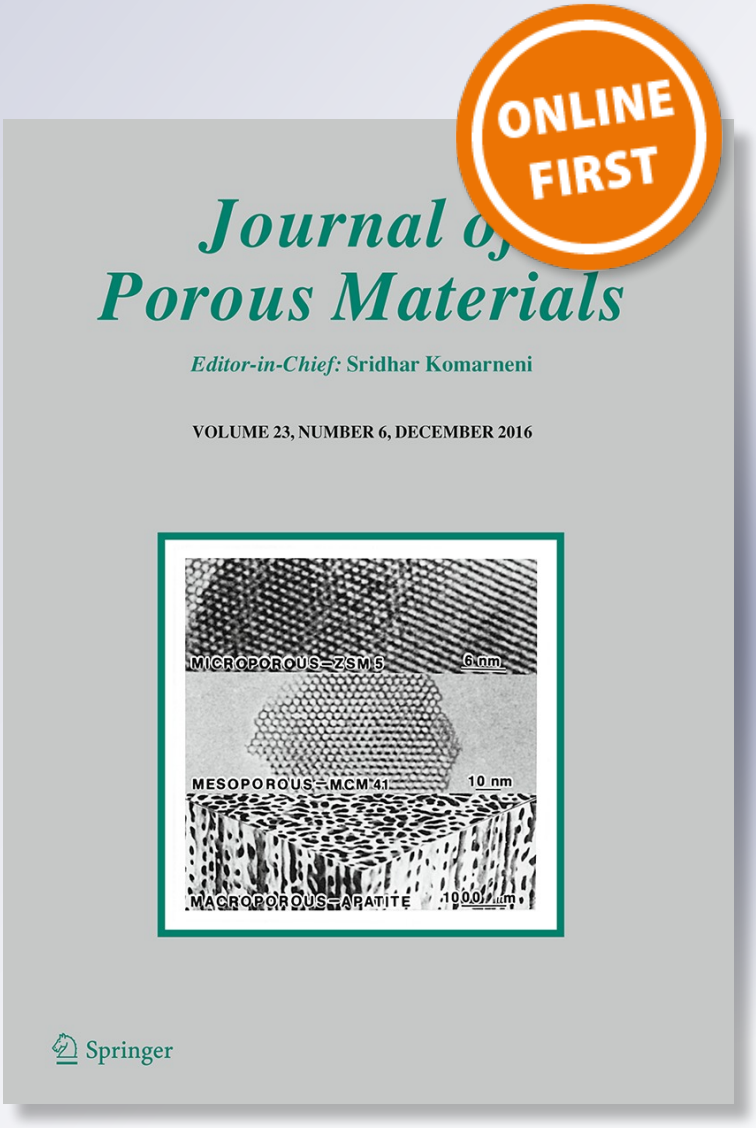

Springer

J Porous Mater
DOI 10.1007/s10934-016-0342-5

Changes in the surface hydrophobicity degree of a MCM-41 used as iron support: a pathway to improve the activity and the olefins production in the Fischer–Tropsch synthesis

N. A. Fellenz[1] · J. F. Bengoa[2] · M. V. Cagnoli[2] · S. G. Marchetti[2]

Abstract The effect of surface hydrophobicity degree of MCM-41 support on activity and selectivity in Fischer–Tropsch synthesis has been studied. The Fe/MCM-41 catalyst was prepared by impregnation of the mesoporous support with iron. A portion of this product was silylated with hexamethyldisilazane. The samples were characterized by atomic absorption spectroscopy, X ray diffraction at low angles, N_2 adsorption at 77 K, Fourier transform infrared spectroscopy and Mössbauer spectroscopy at 25 and 298 K in controlled atmosphere. Catalytic tests were performed simulating industrial operating conditions and showed that the silylated system presents higher activity, lower selectivity toward methane and higher olefin/paraffin ratio. The higher methane production and the lower amount of olefins observed for the non-silylated catalyst indicate that this system has a larger amount of hydrogen on its surface than the silylated one. A detailed discussion about the relationship among surface chemistry, stability, selectivity and the changes in iron species of the catalysts is presented.

Keywords Fe/MCM-41 system · Fischer–Tropsch Synthesis · Olefin production · Silylation treatment · Mössbauer spectroscopy

✉ J. F. Bengoa
bengoajf@quimica.unlp.edu.ar

[1] CONICET, Universidad Nacional de Rio Negro, Sede Atlántica, Belgrano 526, 8500 Viedma, Rio Negro, Argentina

[2] CINDECA, CONICET, CICPBA, UNLP, Fac. Ciencias Exactas, Calle 47, No. 257, 1900 La Plata, Argentina

1 Introduction

The Fischer–Tropsch synthesis (FTS) is a catalytic process used to produce a broad distribution of sulfur-free hydrocarbons (HC) from syngas (mixture of CO and hydrogen with variable composition) which can be represented by the following reaction:

$$(4n + 1)\,H_2 + 2n\,CO \rightarrow C_nH_{2n+2} + C_nH_{2n} + 2n\,H_2O$$

Several metals such as Rd, Ru, Ni, Co and Fe proved to be active as catalysts in FTS. However, for economical reasons only Co and Fe are used as commercial catalysts for industrial processes [1, 2]. Compared to Co, iron based catalysts present many advantages, such as: lower cost, higher availability, higher resistance to poisoning and less methane production. Moreover their selectivity can be easily modified in order to obtain alkenes, oxygenates and/or branched HC [3].

Even though FTS technology has been used for decades to produce HC at industrial scale, reaching a good selectivity towards the desirable products is still a major problem. There is some early evidence in literature, which suggests that the FTS is ''structure sensitive'' [4, 5]. This means that the activity and selectivity of the solid depend on the crystal size of the active phase, generally in the 1–10 nm range. More recently, this property was confirmed using Co and Fe supported catalysts [6–10]. These authors have found that when the crystal size of these species is increased, the catalytic activity and the selectivity to C_{5+} rises, while CH_4 selectivity decreases. Therefore, to control the catalyst selectivity in FTS, the use of particles with a determined average diameter and with a narrow size distribution seems to be a good strategy. To this end, an ''inert'' support with a narrow pore-size distribution and a high thermal stability could be employed.

On the other hand, it should be mentioned that when iron is used as catalyst, water is produced as a by-product, which plays a very important role since it acts as a poison of the iron active phase through an oxidation process [11]. Besides, water favors the progress of "Water–Gas Shift" reaction (WGS).

$$CO + H_2O \leftrightarrow CO_2 + H_2$$

This reaction changes the syngas composition increasing the H_2/CO ratio and thus the selectivity towards methane. Pendyala et al. [12] reported that for iron-based catalysts, a higher amount of water in the fed gas leads to an increase in the rate of the WGS reaction between 10 and 20%. This results in a decrease in the fraction of CO converted into HC and an increase in the methane selectivity.

As mentioned above, a good strategy to increase the selectivity towards to a specific group of products is to obtain a catalyst with a narrow crystal size distribution of the active phase. Small crystals of uniform size could be obtained introducing the iron species precursors inside the channels of a porous support. The MCM-41 material seems to be an interesting support that fulfills all the required characteristics mentioned above. It has average pore sizes between 1.5 and 10 nm depending on the synthesis method, a specific surface area between 900 and 1200 m^2/g and a good thermal stability [13, 14]. These pore diameters inhibit the production of waxes and increase the synthesis of HC in gasoline and diesel range since the chain growth would be limited [6–10]. Nevertheless, these small iron crystals have a lower activity than that of the larger ones due to "intrinsic" effects, since in FTS it can be assumed that, the HC chain growth steps only occur on sites with certain number of metal atoms in a given configuration. The density of these sites might be much lower in small crystallites, rendering them less active [9].

Taking into account all previous considerations, the aim of the present work is to obtain a Fe/MCM-41 catalyst with controlled crystal size of the iron species, avoiding water adsorption over the support surface to hinder the poisoning of the active sites. The prevention of the poisoning was achieved by chemical modification of the catalyst surface compensating the activity decrease due to the small crystal size of the active phase. To this end, a silylation treatment was carried out to eliminate the surface hydroxyls on a Fe/MCM-41 catalyst, increasing its surface hydrophobicity. The effects produced by this treatment on the sample properties were studied by different characterization techniques and their influence on the activity and selectivity on the FTS was tested under similar industrial conditions.

2 Experimental

2.1 Catalyst preparation

The method proposed by Ryoo and Kim [14] was used to synthesize the MCM-41. The pH was controlled during the hydrothermal synthesis. The silica source was sodium silicate and the surfactant used was cetyl-trimethyl-ammonium chloride.

In order to obtain a sample with a nominal iron loading of about 8% w/w, MCM-41 was impregnated with an aqueous solution of iron nitrate using the incipient wetness method. The iron-impregnated solid was dried in air at room temperature (RT), calcined in N_2 flow (60 cm^3/min) from RT up to 603 K (0.2 K/min), and kept at the final temperature for 1 h. This precursor was splitted in two fractions. One of them was named Fe/MCM-41. The other precursor was silylated with hexamethyldisilazane (HMDS) outgassing during 3 h at 573 K ($p_v < 10^{-3}$ Torr). A solution of 1% (v/v) of HMDS in toluene was then prepared in a glove box in Ar atmosphere and added to the dehydrated solids. The mixture was heated at 393 K, for 90 min under stirring. Finally, the treated solid was filtered, washed with 80 cm^3 of toluene, and dried in an oven at 333 K for 16 h. The solid thus obtained was called sil-Fe/MCM-41.

2.2 Catalyst characterization

Atomic absorption spectroscopy (AAS), X ray diffraction (XRD) at low angles, N_2 adsorption at 77 K (BET), Fourier transform infrared spectroscopy (FT-IR), and Mössbauer spectroscopy (MS) at 25 and 298 K were used in sample characterizations.

An AA/AE Spectrophotometer 457 of Laboratory Instrumentation Inc. was used to determine the sample iron loading. The sample was treated in a mixture of HCl and HF up to complete dissolution before measurement.

XRD patterns at low angles were recorded using a standard automated powder X-ray diffraction system Philips PW 1710 with diffracted-beam graphite monochromator, using Cu K_α radiation ($\lambda = 1.5406$ Å) in the range $2\theta = 0.5$–$9°$ with steps of 0.02° and counting time of 2 s/step.

Textural properties: specific surface area (S_g), specific pore volume (V_p) and pore diameter (D_p) were measured in a Micromeritics ASAP 2020 V1.02 E device.

A Bruker IFS66 spectrometer with 1 cm^{-1} resolution by co-addition of 32 scans was used to acquire FT-IR absorption spectra. In order to obtain the corresponding pellets, the samples were mixed with potassium bromide (1:100 ratio).

The Mössbauer spectra were obtained in transmission geometry with a 512-channel constant acceleration spectrometer using a ^{57}Co source (nominally 50 mCi) in

Rh matrix. Velocity calibration was performed versus a 12 μm-thick α-Fe foil. All isomer shifts (δ) are referred to this standard. A Displex DE-202 Closed Cycle Cryogenic System was used to change the temperature between 25 and 298 K. The spectra were folded to minimize geometric effects and fitted using a commercial program with constraints named Recoil [15]. The Mössbauer spectra in controlled atmosphere of the activated catalysts were acquired using the cell described in Ref. [16].

2.3 Activity and selectivity measurements

In order to reproduce the industrial typical operating conditions of FTS, the catalytic tests were carried out during 26 h using a differential reactor at a total pressure of 20 atmospheres (regulated by a back pressure valve) and 543 K, with H_2:CO ratio of 2:1 and a space velocity of 1176 h^{-1} (400 mg catalyst and a total flow of 20 cm^3/min). The precursors were previously activated at a total pressure of 1 atm in H_2:CO = 2:1 flow, heating the sample from 298 to 543 K with a rate of 3.1 K/min. The activated solids were called c-Fe/MCM-41 and c-sil-Fe/MCM-41. The end of this activation procedure was considered as the start of the reaction (zero reaction time). After this treatment, the pressure was set at 20 atm. The syngas mixture was filtered to remove oxygen, water traces and carbonyls before being introduced to the reactor. The tubing lines, downstream of the reactor and before the back pressure valve were kept at about 473 K to avoid the condensation of reaction products, and a trap at 423 K was added to collect the HC higher than C_{20}. After the back pressure valve, the reaction products C_7–C_{19}, heated at 473 K, were analyzed online by gas chromatography using FID detector with HP-1 capillary column. The C_1–C_7 hydrocarbon range was analyzed using another chromatograph connected by a six way valve with the first one, with FID and TCD detectors, using a GS-Gas Pro capillary column and a HAYESEP DB 100/120 packed one, respectively. Between both chromatographs, a condenser at 253 K was used to retain HC higher than C_7. A complete analysis of the products was carried out every two hours.

2.4 Used catalysts characterization

In order to study the structural changes of both catalysts after the FTS by Mössbauer spectroscopy, we have used the cell described in Ref. [16]. This device does not allow working at pressures higher than 1 atm. At 20 atm a higher CO conversion is obtained, consequently, more water quantity is available in the reaction atmosphere and more oxidation of iron species could be expected. However, under our operative conditions, as previously mentioned, the reaction test occurs in a differential reactor with low CO conversion levels (about 2–3%). Therefore, no structural differences between catalysts used at 1 and 20 atm would be expected and these measurements would be representative to understand the differences between both solids.

Our previous studies [17] have demonstrated that after 6 h of reaction at 1 atm the catalyst reaches a pseudo-stationary state. Therefore, the FTS were carried out at 1 atm for 6 h, under the same operative conditions than that used at 20 atm, in this cell. The used catalysts were called us-Fe/MCM-41 and us-sil-Fe/MCM-41.

Besides, the structural characterization of the used catalysts was completed by XRD and FT-IR after exposing the solids to air.

3 Results and discussion

A detailed analysis of the characterization results of the support and the precursors can be found in a previous work [18]. Briefly, the XRD patterns at low angles showed in Fig. 1 indicate that the ordered hexagonal structure of mesoporous MCM-41 remains unchanged after impregnation, calcination and silylation treatments. The textural properties and iron loading are shown in Table 1 and Fig. 2 displays the adsorption–desorption N_2 isotherms for Fe/MCM-41 and sil-Fe/MCM-41 samples. The incorporation of Fe into the MCM-41 support generates a decrease in S_g and V_p in comparison with the support, without substantial changes in D_p. This would imply a partial pore filling of the support with the Fe oxide species. The silylated sample presents a more pronounced decrease of S_g and V_p and additionally, a decrease in D_p. These results were attributed to the covering of the internal pore walls with trimethylsilyl groups. This assumption is consistent with the observed decrease in D_p only for sil-Fe/MCM-41. Similar results were reported by other authors [19, 20]. The C_{BET} values obtained by N_2 adsorption measurements at 77 K are shown in Table 1. Taking into account that the magnitude of C_{BET} is an indication of the adsorption enthalpy between the adsorbate (N_2) and the solid surface, a smaller C_{BET} value would indicate a weaker interaction between N_2 molecules and the solid surface [21]. Besides, the adsorption heat of nitrogen is indeed lower on organic functionalized surfaces than on hydroxyl-rich ones. As a consequence, lower C_{BET} values can be considered as an indication of an increase in the surface hydrophobicity degree due to the coverage by organic groups [22]. Comparing Fe/MCM-41 and sil-Fe/MCM-41 samples, a decrease of 2.4 times in the C_{BET} value can be observed as a consequence of the silylation treatment, which is indicative of the presence of a hydrophobic surface [23, 24]. This result is confirmed by FT-IR results as it will be described below.

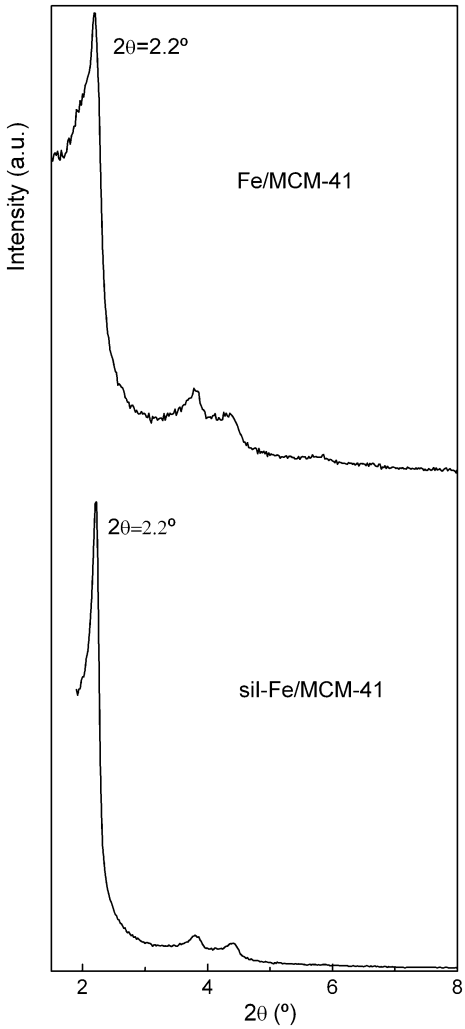

Fig. 1 XRD patterns of Fe/MCM-41 and sil-Fe/MCM-41

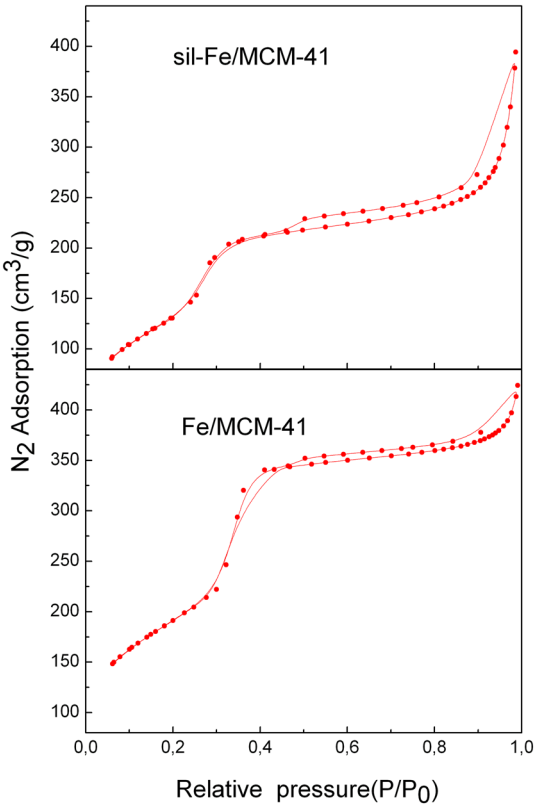

Fig. 2 N_2 adsorption–desorption isotherms for Fe/MCM-41 and sil-Fe/MCM-41

Table 1 Textural properties and iron loading of the studied catalyst samples

Samples	S_g (m^2/g)	D_p(nm)	V_p (cm^3/g)	C_{BET}	%Fe (wt/wt)
MCM-41	912	2.7	0.88	107	–
Fe/MCM-41	691	2.9	0.64	108	8.9 ± 0.4
sil -Fe/MCM-41	494	2.4	0.59	45	8.6 ± 0.4

S_g specific surface area; D_p average pore diameter; V_p specific pore volume; C_{BET} BET model constant

The Mössbauer spectra at RT and 25 K of the precursors are described in Ref. [18]. In both solids, the hyperfine parameters of the signals correspond to two fractions of α-Fe_2O_3 (Table 2) with very different sizes [25]. One of these fractions, consists of crystals of about 36–44 nm located outside the channels of the MCM-41. The majority fraction (about 90%), is constituted by superparamagnetic hematite not magnetically blocked in a complete way even at 25 K. Using the Neel-Brown relaxation model [26] a crystal size of about 3 nm was estimated. Finally, the small doublet that remains at this low temperature can be assigned to paramagnetic Fe^{3+} ions diffused into the MCM-41 walls. Considering this result together with the textural measurements, we can conclude that the iron species are predominantly located inside the MCM-41 channels. Finally, it can be seen that the fitting and the hyperfine parameters obtained at both temperatures [18] are identical for Fe/MCM-41 and sil-Fe/MCM-41 samples –within the experimental error– indicating that the silylation treatment does not modify the nature and size of the iron species.

The solid state ^{29}Si-NMR spectra were shown in a previous work [18] and the FT-IR absorption spectra are shown in Fig. 3. In sil-Fe/MCM-41 the presence of absorption bands can be observed at 759, 850, 2854, 2924 and 2966 cm^{-1} assignable to "stretching" Si–C, "rocking" CH_3–CH_3, symmetric "stretching" of C–H, –CH_3 deformation and non symmetric "stretching" of C–H, respectively [20, 23, 27, 28]. These results confirm the presence of trimethylsilyl groups on this sample. Besides, the broad band centered at about 3500 cm^{-1}, assignable to O–H stretching bands of adsorbed water [29], shows

Table 2 Hyperfine parameters obtained from the Mössbauer spectra at 25 K for activated catalysts

Species	Parameters	c-Fe/MCM-41	c-sil-Fe/MCM-41
Fe_3O_4 Site I	H (T)	52 ± 4	51 ± 3
	δ(mm/s)	0.37(*)	0.37(*)
	2ε (mm/s)	−0.02(*)	−0.02(*)
Fe_3O_4 Site II	H (T)	52 ± 1	52 ± 1
	δ(mm/s)	0.49(*)	0.49(*)
	2ε (mm/s)	0.00(*)	0.00(*)
Fe_3O_4 Site III	H (T)	50 ± 2	50 ± 4
	δ(mm/s)	0.83(*)	0.83(*)
	2ε (mm/s)	−0.27(*)	−0.27(*)
Fe_3O_4 Site IV	H (kOe)	48(*)	48 ± 2
	δ(mm/s)	1.03(*)	1.03(*)
	2ε (mm/s)	−0.41(*)	−0.41(*)
Fe_3O_4 Site V	H (T)	37 ± 2	34 ± 4
	δ(mm/s)	0.96(*)	0.96(*)
	2ε (mm/s)	0.89(*)	0.89(*)
χ-Fe_5C_2 Site I	H (T)	21 ± 8	21 ± 4
	δ(mm/s)	0.30(*)	0.30(*)
	2ε (mm/s)	−0.10(*)	−0.10(*)
χ-Fe_5C_2 Site II	H (T)	26 ± 1	26 ± 2
	δ(mm/s)	0.38(*)	0.38(*)
	2ε (mm/s)	0.30(*)	0.30(*)
χ-Fe_5C_2 Site III	H (T)	13 ± 1	13 ± 1
	δ(mm/s)	0.30(*)	0.30(*)
	2ε (mm/s)	−0.10(*)	−0.10(*)
Fe^{2+} Octahedral	δ(mm/s)	1.6 ± 0.1	1.6 ± 0.1
	Δ(mm/s)	2.2 ± 0.1	2.4 ± 0.1
Fe^{2+} Tetrahedral	δ(mm/s)	1.1 ± 0.1	1.1 ± 0.1
	Δ(mm/s)	2.7 ± 0.1	2.6 ± 0.1

H Hyperfine magnetic field in Tesla; *δ* isomer shift referred to α-Fe at 298 K; *2ε* quadrupole shift; Δ quadrupole splitting

*Parameters held fixed in fitting

a strong reduction in sil-Fe/MCM-41, confirming the higher hydrophobic nature of their surface in concordance with BET results.

Therefore, taking into account all the characterization results, we can conclude that the principal structural difference between both samples is the surface hydrophobicity degree.

Figure 4 shows the Mössbauer spectra at 25 and 298 K of the samples in controlled atmosphere of H_2:CO, after the activation process and subsequent "quenching" to RT. Table 2 displays the hyperfine parameters obtained in fitting.

The spectra at 298 K show an asymmetric doublet with broad lines that could be assigned to paramagnetic and/or superparamagnetic (sp) species, for both catalysts.

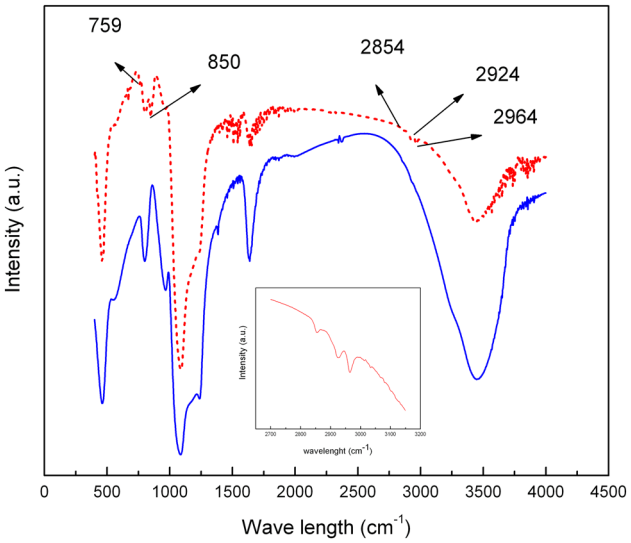

Fig. 3 FT-IR absorption spectra of Fe/MCM-41 (*solid line*) and sil-Fe/MCM-41 (*dash line*). The inset is a magnification of region 2700–3200 cm^{-1} for sil-Fe/MCM-41

In order to carry out a better species assignment, the spectra at 25 K were acquired. The spectra display a curved background, typical of the presence of superparamagnetic relaxation. It is worth noting that, due to the complexity of the spectra, a real fitting was not carried out. The species assignment arises not only from the parameters obtained, but also, from physical and chemical concepts, and the history of the samples. The spectra were fitted with five sextets that corresponds to the five sites of the Fe_3O_4 [30], three sextets assignable to the three sites of χ-Fe_2C_5 carbide [31] and two doublets assignable to Fe^{2+} ions located in octahedral and tetrahedral sites inside the SiO_2 walls [32].

These species are present in the spectra at 298 K in a sp regime: a carbide doublet, a Fe_3O_4 singlet, and two paramagnetic doublets assignable to Fe^{2+} ions diffused inside the SiO_2 walls and/or Fe_3O_4 (sp). The species and their percentages are equal for both catalysts, taking into account the fitting error (Table 3).

The reduction of α-Fe_2O_3 with syngas leads to a quick and complete transformation into Fe_3O_4. A fraction of this magnetite later suffers a transformation into iron carbide [33, 34]. As a result, a mixture of magnetite and iron carbide is present at zero reaction time, avoiding an induction period in the catalytic reaction, as it will be discussed in the following paragraphs. Another interesting phenomenon is that, after the activation treatment, all iron species present at 298 K are sp. It should be borne in mind that the precursors had a small crystal fraction (about 5–8%) magnetically blocked at 298 K, with sizes between 36 and 44 nm located outside the MCM-41 channels. TEM studies of Fe catalysts [35–37], demonstrates

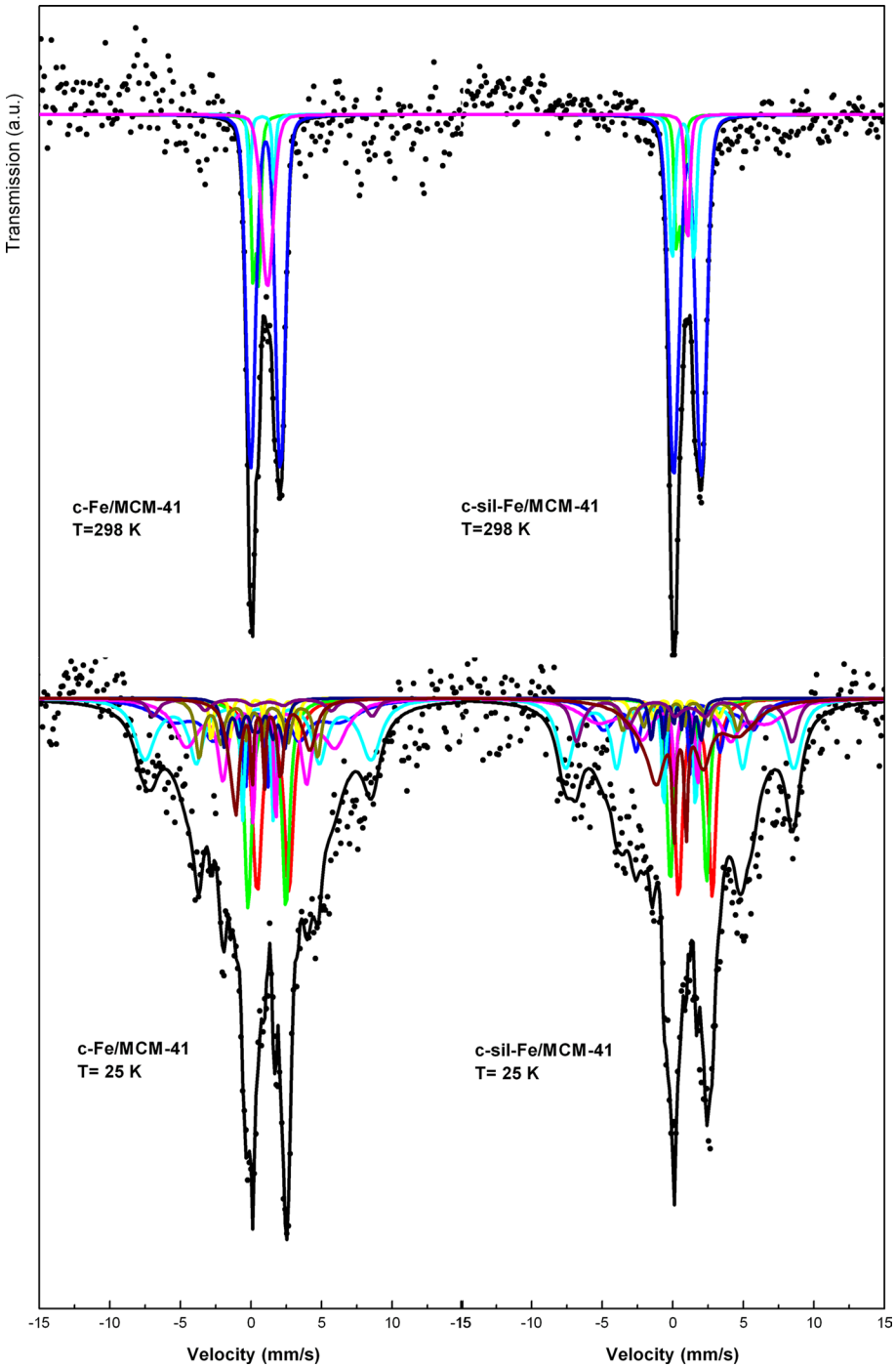

Fig. 4 c-Fe/MCM-41 and c-sil-Fe/MCM-41 Mössbauer spectra at 25 and 298 K in controlled atmosphere of H_2:CO

Table 3 Percentages of different Fe species present in activated catalysts

	Fe_3O_4 (%)	χ-Fe_2O_5 (%)	Fe^{2+} (%)
c-Fe/MCM-41	62 ± 21	13 ± 7	25 ± 4
c-sil-Fe/MCM-41	68 ± 26	10 ± 9	22 ± 4

that iron carbides (FeC_x) grow up on the surface of Fe_3O_4 crystals as small "nodules" when the magnetite is contacted with syngas. Thus, it is possible to conclude that the fraction of bigger crystals of α-Fe_2O_3 leads, in a first stage, to the production of Fe_3O_4 without appreciable size changes. Later, Fe_3O_4 leads to very small nodules of χ carbide with superparamagnetic behavior at 298 K. Similar results were reported for Fe/SBA-15 system by Cano et al. [38].

Table 4 Catalytic tests results at 20 atm after 2, 4 and 24 h of stream

Catalyst	c-Fe/MCM-41			c-sil-Fe/MCM-41		
Time on stream (h)	2	4	24	2	4	24
HC production/g of Fe	13×10^{17}	12×10^{17}	8×10^{17}	14×10^{17}	14×10^{17}	11×10^{17}
CO conversion (%)	3.4	3.2	2.4	3.7	3.6	3.3
S_{CH4} (%)	27	25	22	25	26	17
Olefin/Paraffin up to C_6 without C_1	1.2	0.9	0.7	–	0.9	1.0

Table 4 shows the results of the catalytic tests performed at 20 atm and 543 K with a H_2:CO = 2:1 after 2, 4 and 24 h of stream. It can be seen that sil-Fe/MCM-41 displays approximately 1.4 times higher CO conversion and production of total HC per gram of iron than the non-silylated sample in the pseudo-stationary state. Taking into account that the main difference between both catalysts is the surface hydrophobicity degree, the higher CO conversion and total HC production can be ascribed to the silylation treatment. This effect was observed for cobalt based catalysts supported on amorphous silica by other researchers. For example, Shi et al. [39] reported a higher CO conversion for a Co catalyst with CH_3 modified surface and they associated this behavior to the decrease of the partial pressure of water on the catalyst surface. Ojeda and co-workers [23] reported a similar performance for silylated Co catalyst. They claim that this result is a consequence of superficial water elimination, generating high free active sites available for CO adsorption. On the other hand, analyzing the results at short reaction times (Table 4), it can be seen that both catalysts had similar activities, but then c-Fe/MCM-41 was poisoned faster than c-sil-Fe/MCM-41. This effect could be also attributed to the presence of a higher quantity of water on the non-silylated catalyst surface.

Furthermore, the silylated system presents lower selectivity toward methane and higher olefin/paraffin ratio (Table 4) at the pseudo-stationary state. The difference between CO conversion values of both catalysts prevents a direct analysis of the selectivity parameters, since selectivity comparisons are only valid at iso-conversion conditions. However, considering that a higher CO conversion leads to a higher methane production and a lower olefin/paraffin ratio [40] then, sil-Fe/MCM-41 would produce a higher difference with respect to Fe/MCM-41 if the activity tests would have been realized at iso-conversion conditions. It is well-known that the methane production and the olefin/paraffin ratio in the FTS are associated with the H_2/CO ratio over the catalyst surface. A higher value of this ratio increases the quantity of methane and the selectivity toward to paraffins [41]. Therefore, these results indicate that the non-silylated catalyst has a higher amount of hydrogen on the surface than the silylated one due to a further advance of WGS reaction. This fact can be attributed to a greater quantity of water molecules on the surface of the non-silylated system, in agreement with the discussion of the activities results. The changes in the methane production and olefin/paraffin ratio, at the beginning of the reaction, would also reflect a faster increase in the water content on the non-silylated solid, producing a higher progress of the WGS.

Figure 5 shows the selectivity histograms of both catalysts. The products were grouped in different fractions according to their industrial applications: light HC (C_2–C_4), gasoline (C_5–C_{12}), diesel (C_{13}–C_{18}) and soft waxes (C_{19+}). It can be seen that sil-Fe/MCM-41 catalyst produces higher quantities of heavy HC, especially in the diesel and soft waxes fractions. Again, this finding could be assigned to the presence of a lower H_2/CO ratio at the catalyst surface, producing a lower termination reaction favoring the chain growth. This is an important result, which indicates that the incorporation of trimethylsilyl groups in the Fe/MCM-41 system generates a significant improvement in the heavy HC production in the FTS at 20 atm. This behavior is more evident at longer reaction times.

To analyze the structural changes in MCM-41 supports after FTS, the XRD spectra were obtained at low angles of the catalysts used at 1 atm, for 6 h (Fig. 6). The characteristic peaks of an ordered mesoporous solid MCM-41

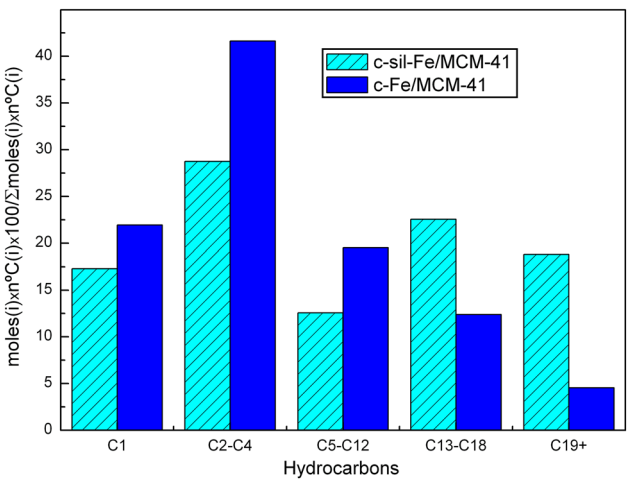

Fig. 5 selectivity histograms of c-Fe/MCM-41 and c-sil-Fe/MCM-41 catalysts after 24 h of stream

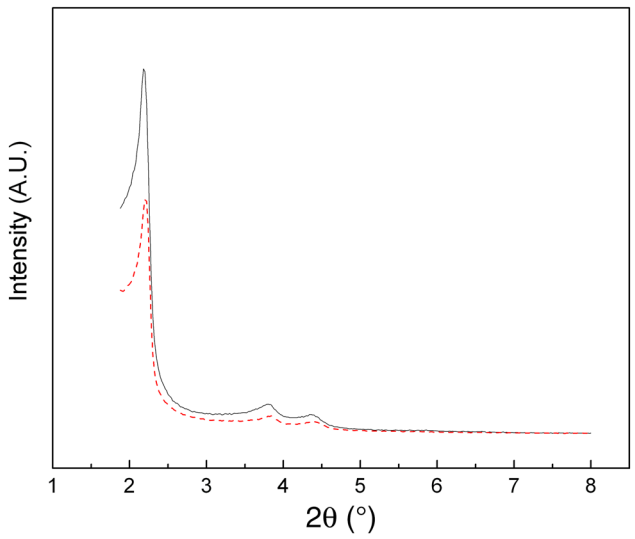

Fig. 6 low angles XRD spectra of used catalysts. c-Fe/MCM-41 solid line, c-sil-Fe/MCM-41 dash line

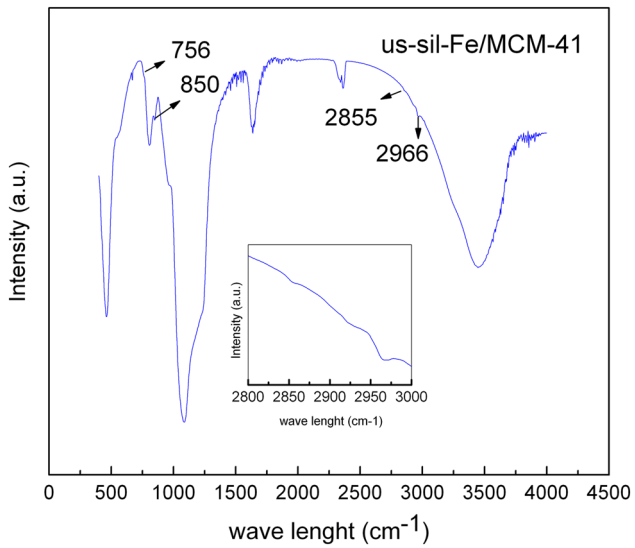

Fig. 7 infrared spectrum of us-sil-Fe/MCM-41. The *inset* is a magnification of region 2800–3000 cm^{-1}

can be observed. In both samples the structure was stable in these reaction conditions. The position of the more intense peak at $2\theta = 2.2°$ is the same in both solids, indicating that the structural parameter a_0 (distance between centers of neighboring pores) and d_{100} (interplanar spacing calculated for the most intense peak) did not change after the FTS.

The stability of the trimethylsilyl groups under reaction conditions was evaluated by FTIR after using the silylated catalyst during 6 h in FTS. The infrared spectrum of us-sil-Fe/MCM-41 is shown in Fig. 7. The bands previously described for sil-Fe/MCM-41 remain, indicating the presence of trimethylsilyl groups on the catalyst surface after 6 h of reaction. A slight intensity decrease is observed.

Finally, the Mössbauer spectra in controlled atmosphere of (H_2:CO) at 30 and 298 K were acquired after 6 h of reaction and subsequent "quenching" (Fig. 8).

At 298 K the spectra displays a very intense central signal for both catalysts. An asymmetric doublet with very broad lines is observed in us-Fe/MCM-41, while the superposition of three lines with different intensities can be seen in us-sil-Fe/MCM-41. In all cases, these signals could be assigned to paramagnetic and/or sp species. Besides, two sextets of low intensity are also observed. In order to assign the central signals, the spectra were acquired at 30 K. Unlike the fresh catalysts, the spectra background is not curved, indicating that all magnetic species are completely blocked. For this reason, the fitting was carried out with hyperfine field distributions, without superparamagnetic relaxation. The spectrum of us-Fe/MCM-41 was fitted with two doublets and five sextets, while an additional sextet was necessary for us-sil-Fe/MCM-41. Table 5 displays the hyperfine parameters obtained in fitting.

The two doublets were assigned to Fe^{2+} ions located in tetrahedral (lower δ and Δ) and octahedral sites inside the SiO_2 walls, in a similar way to that for the activated catalyst. These sites were called Q_1 and Q_2, respectively, by Clausen et al. [32]. The δ value for Fe^{2+} located in Q_1 sites is near to the value of a Fe^{3+}. These sites seem to have higher trend to re-oxidize in contact with the FTS atmosphere.

Only two sextets were used to fit the signals assignable to Fe_3O_4. One of them represents the "weighted" average of the different Fe^{3+} sites, and the other the "weighted" average of the different Fe^{2+} sites [30]. This methodology was chosen bearing in mind that the Fe_3O_4 percentage diminishes in comparison with the activated catalysts (from 62 to 17% in us-Fe/MCM-41, and from 68 to 32% in us-sil-Fe/MCM-41). Therefore, considering that the signal is not as well defined as in the activated catalysts, it is not recommended to use the five interactions belonging to the different crystals sites of the Fe_3O_4.

The remaining three sextets were assigned to I, II and III sites of χ-Fe_5C_2 carbide [31]. Taking into account that at $H \approx 25$ T the II site of χ-Fe_5C_2 carbide and the I site of ε′-$Fe_{2.2}C$ carbide exhibit overlapped signals, the presence of the latter carbide cannot be discarded [42]. However, the II site of ε′-$Fe_{2.2}C$ ($H = 19$ T) was only detected in us-sil-Fe/MCM-41. This site was not detected in us-Fe/MCM-41, probably due to the very low total content of carbide in this sample.

All iron species mentioned above are also present in the spectra at 298 K: a doublet of sp carbide, two doublets of Fe^{2+} assignable to ions that have diffused inside the SiO_2

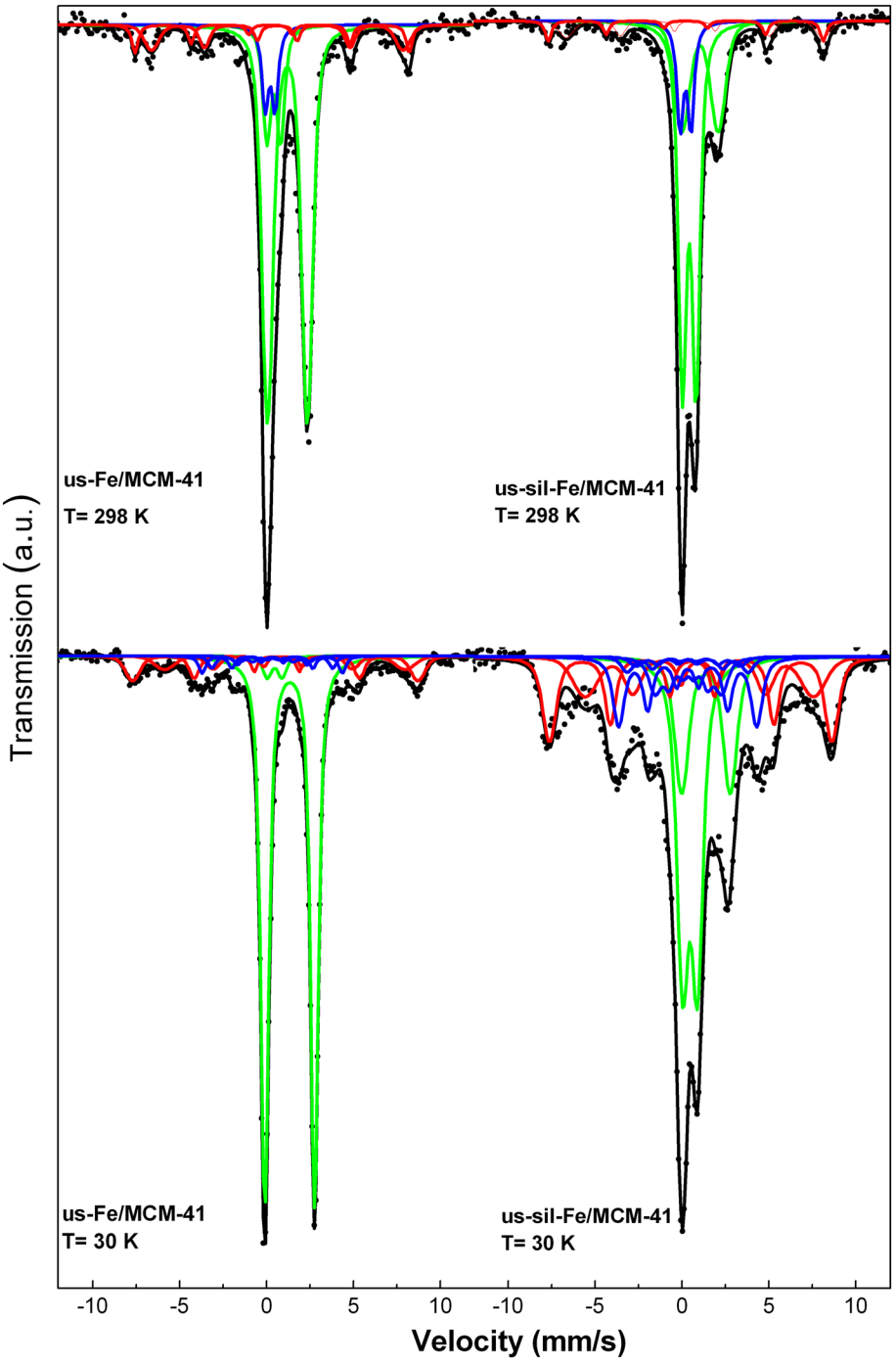

Fig. 8 Used catalysts Mössbauer spectra at 30 and 298 K in controlled atmosphere of H_2:CO

walls and/or Fe_3O_4 (sp), one sextet of Fe^{3+} located in tetrahedral sites and another sextet of $Fe^{\text{“2.5+”}}$ ions located in octahedral sites of Fe_3O_4 [43].

The activated catalysts have the same iron species, with equal percentages and crystal sizes; they only differ in their surface characteristics. However, used catalysts have experienced important changes in their structural properties (Table 6). First, in both samples the initial Fe_3O_4 percentage diminishes. For the c-Fe/MCM-41 sample, the decrease in magnetite content leads to an extraordinary increase in the amount of Fe^{2+} diffused into the SiO_2 walls (about 200% in comparison with the activated catalyst), while for sil-Fe/MCM-41 this increase was about 100%. On the other hand, the silylated sample has a higher content of carbides. These results indicate that both catalysts experienced structural changes during the FTS and that they contain mobile species, especially the Fe^{2+} ions. The tendency of these ions to diffuse inside the walls is more pronounced in the

Table 5 Hyperfine parameters of used catalysts during 6 h in FTS obtained from fitting of Mössbauer spectra at 30 K

Species	Parameters	us-Fe/MCM-41	us-sil-Fe/MCM-41
Fe_3O_4 Sites (I + II + III)	H (T)	51 ± 1	50 ± 1
	δ(mm/s)	0.55(*)	0.55(*)
	2ε (mm/s)	−0.09(*)	−0.09(*)
Fe_3O_4 Sites (IV + V)	H (T)	43 ± 1	41 ± 1
	δ(mm/s)	1.0(*)	1.0(*)
	2ε (mm/s)	0.11(*)	0.11(*)
χ-Fe_5C_2 Site I	H (T)	22 ± 1	22(*)
	δ(mm/s)	0.33(*)	0.33(*)
	2ε (mm/s)	0.0(*)	0.0(*)
χ-Fe_5C_2 Site II + ε`-$Fe_{2.2}C$ Site I	H (T)	25 ± 1	25 ± 1
	δ(mm/s)	0.33(*)	0.33(*)
	2ε (mm/s)	0.0(*)	0.0(*)
χ-Fe_5C_2 Site III	H (T)	13 ± 1	12 ± 1
	δ(mm/s)	0.37(*)	0.37(*)
	2ε (mm/s)	0.0(*)	0.0(*)
ε′-$Fe_{2.2}C$ Site II	H (T)	n.d	186(*)
	δ(mm/s)	n.d	0.36(*)
	2ε (mm/s)	n.d	0.0(*)
Fe^{2+} in octahedral Site	δ(mm/s)	1.3 ± 0.1	1.4 ± 0.1
	Δ(mm/s)	2.9 ± 0.1	2.8 ± 0.1
Fe^{2+} in tetrahedral Site	δ(mm/s)	0.47(*)	0.5 ± 0.1
	Δ(mm/s)	0.86(*)	0.9 ± 0.1

H Hyperfine magnetic field in Tesla; *δ* isomer shift referred to α-Fe at 298 K; *2ε* quadrupole shift; *Δ* quadrupole splitting,. *n.d* no detected

*Parameters held fixed in fitting

Table 6 Percentages of different Fe species present in catalysts used 6 h in FTS

	Fe_3O_4 (%)	χ-Fe_5C_2 + ε′-$Fe_{2.2}C$ (%)	Fe^{2+} (%)
us-Fe/MCM-41	17 ± 2	9 ± 2	74 ± 2
us-sil-Fe/MCM-41	32 ± 2	24 ± 5	44 ± 2

non-silylated system. Bearing in mind that the activated catalysts only differ in the surface hydrofobicity degree, it could be speculated that the presence of water adsorbed on the surface of c-Fe/MCM-41, by-product of the FTS, acts as a mobilization "vector" for the Fe^{2+} ions, favoring their introduction into octahedral and tetrahedral sites of the SiO_2 lattice.

It should be mentioned that the iron species diffused inside the support walls, due to their inaccessibility, are catalytically inactive. For this reason, it is evident that a quick expulsion from the catalyst surface of the water produced in the synthesis is essential to reach a high catalytic activity. This process is carried out by the trimethylsilyl groups located inside the channels of the support in c-sil-Fe/MCM-41. Taking into account that 6 h of reaction are enough to achieve the pseudo steady-state, it can be concluded that the Fe^{2+} ions diffusion is a fast process.

Another interesting result is that, after using the catalysts, a magnetically blocked fraction appears at 298 K with a percentage very close to that detected in the precursor (about 12–15%) for the α-Fe_2O_3 crystals located on the external surface. However, in these used catalysts, this fraction corresponds to Fe_3O_4 instead of α-Fe_2O_3. It should be borne in mind that during the activation treatment this fraction has disappeared due to the production of very small carbide "nodules" with sp behavior. It could be inferred that when the catalyst is "working", these carbide "nodules" are re-oxidized, leading to the appearance of bigger Fe_3O_4 crystals. It can be speculated that during this re-oxidation a sintering of the carbide "nodules" occurs and magnetite crystals with similar sizes to the original α-Fe_2O_3 are produced. Depending on the conversion degree, H_2O/H_2 and CO_2/CO ratios can be changed. As a consequence, the reaction atmosphere can produce a reduction or an oxidation of the surface iron species of the catalysts [44]. The present results would indicate that under our reaction conditions, the atmosphere is oxidant for both catalysts.

4 Conclusions

MCM-41 mesoporous solid was used as iron support to produce HC through the FTS. In order to study the effect of the hydrophobicity of the support surface, one fraction of the nanocomposite Fe/MCM-41 was subjected to a silylation treatment incorporating trimethylsilyl groups onto its pores surface. The reaction conditions were selected in order to simulate operative industrial conditions with a differential reactor. Both activated catalysts had the same iron species, with equal percentages and crystal sizes; they only differ in their surface characteristics.

Under reaction conditions, the silylated catalyst displays higher CO conversion, higher production of total HC per gram of iron and higher chain growth in the pseudo-stationary state. Taking into account that the only difference between both catalysts is the surface hydrophobicity degree, these experimental observations would be consequence of the silylation treatment. Besides, the silylated system presents lower selectivity toward methane and higher olefin/paraffin ratio. All these experimental observations would indicate that the water molecules, by-product of the FTS, are desorbed faster from the actives sites in the silylated catalyst. The quick water expulsion produces three benefits:

- More free active sites for CO conversion.
- The WGS reaction advance is hindered; therefore the H_2/CO ratio is not increased and the hydrogenating capacity decreases.
- The diffusion of the Fe^{2+} ions into the support walls was relented to some extent due to the fact that water acts as a mobilization vector for the Fe^{2+} ions towards the octahedral and tetrahedral sites of the SiO_2 network. In this way, the loss of the active iron species is smaller.

Acknowledgements The authors acknowledge the financial support for this research provided by Universidad Nacional de Río Negro (PI 40 C-392), Consejo Nacional de Investigaciones Científicas y Técnicas (CONICET PIP 00547), Comisión de Investigaciones Científicas de la Provincia de Buenos Aires (CICPBA) and Universidad Nacional de La Plata. We also wish to thank to Ms Valle Graciela for FTIR measurements and Juan Julio and Martín Ramón for its assistance in electronic devices. The authors are grateful to María Cecilia Moreno, CICPBA translator, for checking the English version.

References

1. M. Luo, B.H. Davis, Appl. Catal. A. Gen. **246**, 171–181 (2003). doi:10.1016/S0926-860X(03)00024-3
2. M. Luo, H. Hamdeh, B.H. Davis, Catal. Today. **140**, 127–134 (2009). doi:10.1016/j.cattod.2008.10.004
3. R.J. O'Brien, L. Xu, R.L. Spicer, S. Bao, D.R. Milburn, B.H. Davis, Catal. Today. **36**, 325–334 (1997). doi:10.1016/S0920-5861(96)00246-5
4. M. Boudart, A. Delbouille, J.A. Dumesic, S. Khammouma, H. Topsøe, J. Catal. **37**, 486–502 (1975). doi:10.1016/0021-9517(75)90184-0
5. M.A. Mc Donald, D.A. Storm, M. Boudart, J. Catal. 102, 386–400 (1986). doi:10.1016/0021-9517(86)90175-2
6. E.I. Mabaso, E. van Steen, M. Caléis, DGMK/SCI-Conference "Synthesis gas chemistry", October, (Dresden, Germany, 2006), pp. 4–6
7. G.L. Bezemer, J.H. Bitter, H.P.C.E. Kuipers, H. Oosterbeek, J.E. Holewijn, X. Xu, F. Kapteijn, A.J. van Dillen, K.P. de Jong, J. Am. Chem. Soc. **128**(12), 3956–3964 (2006). doi:10.1021/ja058282w
8. J.-Y. Park, Y.-J. Lee, P.K. Khanna, K.-W. Jun, J.W. Bae, Y.H. Kim, J. Mol. Catal. A. Chem. **323**, 84–90 (2010). doi:10.1016/j.molcata.2010.03.025
9. R.A. van Santen, M.M. Ghouri, S. Shetty, E.M.H. Hensen, Catal. Sci. Technol. **1**, 891–911 (2011). doi:10.1039/C1CY00118C
10. N. Fischer, E. van Steen, M. Claeys, J. Catal. **299**, 67–80 (2013). doi:10.1016/j.jcat.2012.11.013
11. A.K. Dalai, T.K. Das, K.V. Chaudhari, G. Jacobs, B.H. Davis, Appl. Catal. A. **289**, 135–142 (2005). doi:10.1016/j.apcata.2005.04.045
12. V.R.R. Pendyala, G. Jacobs, J.C. Mohandas, M. Luo, W. Ma, M.K. Gnanamani, B.H. Davis, Appl. Catal. A. **389**, 131–139 (2010). doi:10.1016/j.apcata.2010.09.018
13. J.S. Beck, J.C. Vartuli, W.J. Roth, M.E. Leonowicz, C.T. Kresge, K.D. Schmitt, C.T.W. Chu, D.H. Olson, E.W. Sheppard, J. Am. Cem. Soc. **114**, 10834–10843 (1992). doi:10.1021/ja00053a020
14. R. Ryoo, J.M. Kim, J. Chem. Soc. Chem. Commun. 711–712 (1995). doi:10.1039/C39950000711
15. K. Lagarec, D.G. Rancourt, *"Mössbauer spectral analysis software" Dep. of Phys*, Version 1.0. (University of Otawa, Ottawa, 1998)
16. I. Pérez De Berti, J. Bengoa, N. Fellenz, R. Mercader, S. Marchetti, Rev. Sci. Instrum. **86**, 023903-1-023903-5 (2015). doi:10.1063/1.4913382
17. N.A. Fellenz, PhD Thesis, http://hdl.handle.net/10915/2755
18. N.A. Fellenz, J.F. Bengoa, S.G. Marchetti, A. Gervasini, Appl. Catal. A. Gen. **435–436**, 187–196 (2012). doi:10.1016/j.apcata.2012.06.003
19. R.R. Sever, R. Alcala, J.A. Dumesic, T.W. Root, Microporous Mesoporous Mater. **66**, 53–67 (2003). doi:10.1016/j.micromeso.2003.08.019
20. X.S. Zhao, G.Q. Lu, J. Phys. Chem. B. **102**, 1556–1561 (2008). doi:10.1021/jp972788m
21. R. Mariscal, M. López-Granados, J.L.G. Fierro, J.L. Sotelo, C. Martos, R. Van Grieken, Langmuir. **16**, 9460–9467 (2000). doi:10.1021/la000876j
22. D. Brunel, A. Cauvel, F. Fajula, F. DiRenzo, in *Zeolites: a refined tool for designing catalytic sites*, ed. by B. Delmon, J.T. Yates. Studies in surface science and catalysis, vol. 97 (Elsevier, Amsterdam, 1995), p. 173–180. doi:10.1016/S0167-2991(06)81887-2
23. M. Ojeda, F.J. Pérez-Alonso, P. Terreros, S. Rojas, T. Herranz, M. López Granados, J.L. García Fierro, Langmuir. **22**, 3131–3137 (2006). doi:10.1021/la052980c
24. J.M. Rosenholm, M. Lindén, Chem. Mater. **19**, 5023–5034 (2007). doi:10.1021/cm071289n
25. E. Murad, J.H. Johnston, in *Mössbauer Spectroscopy Applied to Inorganic Chemistry*, vol. 2, ed. G.J. Long, (Plenum Publishing Corporation, New York 1987)
26. W.F. Brown Jr., Phys. Rev. **130**, 1677 (1963). doi:10.1103/PhysRev.130.1677
27. J. Joo, T. Hyeon, J. Hyeon-Lee, Chem. Commun. 1487–1488 (2000). doi:10.1039/B001886O.
28. J. Ryczkowski, J. Goworek, W. Gac, S. Pasieczna, T. Borowiecki, Thermochimica Acta **434**, 2–8 (2005). doi:10.1016/j.tca.2004.12.020
29. A. Calvo, P.C. Angelomé, V.M. Sánchez, D.A. Scherlis, F.J. Williams, G.J.A.A. Soler-Illia, Chem. Mater. **20**, 4661–4668 (2008). doi:10.1021/cm800597k
30. F.J. Berry, S. Skinner, M.F. Thomas, J. Phys. Condens. Matter. **10**, 215–220 (1998). doi:10.1088/0953-8984/10/1/024
31. S.-C. Lin, J. Phillips, J. Appl. Phys. **58**(5), 1943–1949 (1985). doi:10.1063/1.336001
32. B.S. Clausen, H. Topsøe, S. Mørup, Appl. Catal. **48**, 327–340 (1989). doi:10.1016/S0166-9834(00)82802-X
33. S. Li, G.D. Meitzner, E. Iglesia, J. Phys. Chem. B. **105**, 5743–5750 (2001). doi:10.1021/jp010288u
34. S. Li, W. Ding, G.D. Meitzner, E. Iglesia, J. Phys. Chem. B. **106**, 85–91 (2002). doi:10.1021/jp0118827
35. N.B. Jackson, A.K. Datye, L. Mansker, R.J. O'Brien, B.H. Davis, Stud. Surf. Sci. Catal. **111**, 501 (1997)
36. M.D. Shroff, D.S. Kalakkad, K.E. Coulter, S.D. Köhler, M.S. Harrington, N.B. Jackson, A.G. Sault, A.K. Datye, J. Catal. **156**, 185–207 (1995). doi:10.1006/jcat.1995.1247
37. J. Xu, C.H. Bartholomew, J. Phys. Chem. B. **109**, 2392–2403 (2005). doi:10.1021/jp048808j
38. L.A. Cano, M.V. Cagnoli, J.F. Bengoa, A.M. Alvarez, S.G. Marchetti, J. Catal. **278**, 310–320 (2011). doi:10.1016/j.jcat.2010.12.017
39. L. Shi, J. Chen, K. Fang, Y. Sun, Fuel **87**, 521–526 (2008). doi:10.1016/j.fuel.2007.03.018
40. M. Röper, *Fischer–tropsch synthesis, catalysis in C1 chemistry*, ed. W. Keim, **4**, 41 (1983)

41. Y. Liu, B-T. Teng, X-H. Guo, Y. Lia, J. Chang, L. Tian, X. Hao, Y. Wang, H-W. Xiang, Y-Y. Xu, Y-W. Li, J. Molec. Catal. A. Chem **272**, 182–190 (2007). doi:10.1016/j.molcata.2007.03.046
42. M. Pijolat, V. Perrichon, P. Bussiére, J. Catal. **107**, 82–91 (1987). doi:10.1016/0021-9517(87)90274-0
43. R.E. Vandenberghe, E. De Grave, C. Landuydt, L.H. Bowen, Hyperfine Inter. **53**, 175–196 (1990). doi:10.1007/BF02101046
44. S.-J. Liaw, B.H. Davis, Topics Catal. **10**, 133–139 (2000). doi:10.1023/A:1019176403861